

Search for the intermediate Mass Higgs Signal at TeV $e\gamma$ colliders

Kingman Cheung

Dept. of Physics & Astronomy, Northwestern University, Evanston, Illinois 60208, USA

ABSTRACT

The intermediate mass Higgs (IMH) can be abundantly produced through the process $e^-\gamma \rightarrow W^-H\nu$ at TeV $e^-\gamma$ colliders, which are realized by the laser back-scattering method. We search for the signature of $W^-H \rightarrow (jj)(b\bar{b})$ plus missing transverse momentum, with and without considering the b -tagging. We also analyse all the potential backgrounds from $e^-\gamma \rightarrow W^-Z\nu, W^-W^+e^-, ZZ e^-, \bar{t}b\nu$ and $t\bar{t}e^-$. With our selective acceptance cuts these backgrounds are reduced to a manageable level. We find that for the entire intermediate mass range 60 – 150 GeV the Higgs discovery should be viable. We also present detail formulas for the helicity amplitudes of these processes.

Pacs: 14.80.Gt, 14.80.Er, 13.60.Fz

I. INTRODUCTION

The symmetry-breaking sector of the standard model (SM) is the most mysterious part of the particle theory. Even for the simplest minimal SM the Higgs boson, which is responsible for the symmetry-breaking, has not yet been found, and there is no theoretical restriction on its mass except the unitarity implies an upper limit of about 1 TeV on its mass. The discovery of the Higgs boson depends on its mass, which determines the decay channel to search for. For the heavy Higgs ($m_H \gtrsim 2m_Z$) we can use the gold-plated channel, $H \rightarrow ZZ \rightarrow \ell\bar{\ell}\ell\bar{\ell}$ to identify it at hadronic colliders [1], and even the four-jet mode of $H \rightarrow ZZ, WW \rightarrow (jj)(jj)$ at e^+e^- colliders [2,3]. The present lower bound on m_H from LEP is about 52 – 53 GeV [4], which can extend up to 60 GeV in near future. There remains a mass range of 60 to 140 GeV that the Higgs, which predominately decays into $b\bar{b}$ pair, could be difficult to identify because of large hadronic background at hadronic colliders. Recent studies showed that we can use the rare photonic mode of IMH decaying into $\gamma\gamma$ to search for the Higgs boson in the direct $gg \rightarrow H$ [5] production, or in the associated productions with W -boson [6] or $t\bar{t}$ pair [7]. While at e^+e^- colliders, we can use the $e^+e^- \rightarrow ZH \rightarrow (f\bar{f})b\bar{b}$ to identify the IMH upto about 90 – 95 GeV at LEP II [8], and the whole intermediate mass range at Next Linear Collider (NLC) [8].

With the recent discussions of converting the linear e^+e^- colliders into $\gamma\gamma$ or $e\gamma$ colliders by laser back-scattering method, they provide new physics possibilities of detecting and probing the properties of the Higgs boson [9]. With a 0.5 TeV e^+e^- collider in $\gamma\gamma$ mode, the Higgs production by photon-photon fusion via a triangular loop of heavy fermions and W -boson can be used to discover a heavy Higgs boson ($m_H > 2m_Z$) [9,10,11]. It was shown in Ref. [11] that a heavy Higgs boson of mass up to about 350 GeV should be able to be identified in the decay mode of $H \rightarrow ZZ \rightarrow q\bar{q}\ell\bar{\ell}$, which has a sufficiently large branching fraction and is free from the huge $\gamma\gamma \rightarrow WW$ background. It was also shown in Ref. [11] that the detectability in general decreases for a higher energy machine. On the other hand, the process $\gamma\gamma \rightarrow t\bar{t}H$ [12] is shown to be better than the corresponding process, $e^+e^- \rightarrow t\bar{t}H$,

in e^+e^- collider for the measurement of the Yukawa top-Higgs coupling at $\sqrt{s} = 1 - 2$ TeV.

Another interesting Higgs production process is $e\gamma \rightarrow WH\nu$ [13,14] by colliding a photon beam with an electron or positron beam. The cross section of this process is shown to be comparable to $e^+e^- \rightarrow \nu\bar{\nu}W^*W^* \rightarrow \nu\bar{\nu}H$ at $\sqrt{s} = 1 - 2$ TeV, and much larger than the Bjorken process $e^+e^- \rightarrow ZH$ for IMH mass range. However, the backgrounds have not fully analysed. The major backgrounds for IMH search in the process $e^-\gamma \rightarrow W^-H\nu$ come from $e^-\gamma \rightarrow W^-Z\nu$, WWe^- and ZZe^- , in which the boson-pair decay hadronically into four jets in the final state. Also there are backgrounds from $e^-\gamma \rightarrow b\bar{t}\nu \rightarrow b\bar{b}W^-\nu$ and $e^-\gamma \rightarrow t\bar{t}e^- \rightarrow b\bar{b}WWe^-$. With the b -identification these backgrounds can be much reduced, however, the b -tagging efficiency is so far uncertain. It is then the purpose of this paper to investigate the feasibility of identifying the IMH through the process $e^-\gamma \rightarrow W^-H\nu$ at TeV $e\gamma$ colliders, with and without implementing the b -tagging. The organization is as follows: we will describe the calculation of the signal and background processes including the photon luminosity function in Sec. II, following which the results will be presented in according to the case of with and without implementing b -tagging in Sec. III. We will then summarize the conclusions and discussions in Sec. IV. We will also give detail formulas for the processes involved in the Appendix A.

II. CALCULATION METHODS

A. Photon luminosities

We use the energy spectrum of the back-scattered photon given by [15]

$$F_{\gamma/e}(x) = \frac{1}{D(\xi)} \left[1 - x + \frac{1}{1-x} - \frac{4x}{\xi(1-x)} + \frac{4x^2}{\xi^2(1-x)^2} \right], \quad (1)$$

where

$$D(\xi) = \left(1 - \frac{4}{\xi} - \frac{8}{\xi^2}\right) \ln(1 + \xi) + \frac{1}{2} + \frac{8}{\xi} - \frac{1}{2(1 + \xi)^2}, \quad (2)$$

$\xi = 4E_0\omega_0/m_e^2$, and ω_0 is the energy of the incident laser photon. $x = \omega/E_0$ is the fraction of the energy of the incident positron carried by the back-scattered photon, and the maximum value x_{\max} is given by

$$x_{\max} = \frac{\xi}{1 + \xi}. \quad (3)$$

The value for ξ is chosen in such a way that the back-scattered photon will not produce the unwanted e^+e^- pairs with the incident laser photon. We choose ξ to be 4.8, and so $x_{\max} \simeq 0.83$, $D(\xi) \simeq 1.8$, and $\omega_0 = 1.25(0.63)$ eV for a 0.5(1) TeV e^+e^- collider. Here we have assumed that the positron and the back-scattered photon beams are unpolarized. We also assume that, on average, the number of the back-scattered photons produced per positron is 1.

Besides, photon is also known to interact via its quark and gluon constituents [16]. This is referred as a ‘‘resolved’’ photon process. The gluons and quarks are treated as partons inside the photon with the distribution functions $P_{i/\gamma}(x)$ to describe the probability that the parton i carries a momentum fraction x . What we need is the gluon distribution function to calculate some backgrounds wherever the electron-gluon scattering also contributes in the case of electron-photon scattering. However, the gluon parton distribution function inside photon has large uncertainty because limited experimental data are available. We choose the parameterization of Drees and Grassie (DG) [17] for the photon structure function, a scale $Q^2 = \hat{s}/4$ and Λ_4 to be 0.4 GeV for both the photon structure function and α_s (evaluated at the second order).

The subprocess cross sections $\hat{\sigma}$ must be folded with the luminosities to find the total cross sections. In case of electron-photon scattering, the cross section σ is

$$\sigma(s) = \int_{x_{1min}}^{x_{max}} dx_1 F_{\gamma/e}(x_1) \hat{\sigma}(\hat{s} = x_1 s). \quad (4)$$

For the electron-gluon scattering the total cross section is given by

$$\sigma(s) = \int_{x_{1min}}^{x_{max}} dx_1 \int_{x_{2min}}^1 dx_2 F_{\gamma/e}(x_1) P_{g/\gamma}(x_2) \hat{\sigma}(\hat{s} = x_1 x_2 s). \quad (5)$$

B. $e\gamma \rightarrow WH\nu$

The contributing Feynman diagrams are shown in Fig. 1. This process has been calculated in details in Refs. [13,14]. For completeness detail formulas for the matrix elements are given in Appendix A. We did an independent calculation that agrees with their results. The gluon parton inside photon does not contribute because the gluon does not couple to either initial or final state particles. For the Higgs in the intermediate mass range the signature, due to the dominate decay of $H \rightarrow b\bar{b}$ and the hadronic decay of W , will be

$$e^- \gamma \rightarrow W^- H \nu \rightarrow (jj)(b\bar{b})\nu, \quad (6)$$

where there are four jets plus missing energy in the final state. Two of the four jets are reconstructed at the W mass, and the other two can be reconstructed as a resonance peak at the Higgs mass. For this signature the direct backgrounds are the W^-Z , W^-W^+ and ZZ productions where the W and Z decay hadronically into four jets, especially if the Higgs mass is close to W or Z mass. These processes will be described next.

C. $e^- \gamma \rightarrow W^- Z \nu$, $W^- W^+ e^-$ **and** ZZe^-

These processes have been calculated in Ref. [18]. There are totally 11 contributing Feynman diagrams in the process $e^- \gamma \rightarrow W^- Z \nu$, 18 in $e^- \gamma \rightarrow W^- W^+ e^-$, and 6 in $e^- \gamma \rightarrow ZZe^-$, in the general R_ξ gauge, shown in Fig. 2. The W^-Z and W^-W^+ productions are interesting by their own in the subject of probing the triple and quartic gauge-boson interactions [18]. The formulas for the Feynman amplitudes of these processes are presented here again in Appendix A. The WW production starts with a high cross section (see Fig. 4), but it was shown in Ref. [18] that a transverse momentum $p_T(VV)$ cut on the boson pair can reduce the W^-W^+ background substantially, and only moderately on the signal and W^-Z . Also we will show that the central electron vetoing method will be very useful in further reducing the WW background. The W^-W^+ background is reducible if 100% b -tagging is used, since we can require $b\bar{b}$ pair in the final state. The W^-W^+ background decaying into

b and \bar{b} is well suppressed by the Cabbibo angle. Otherwise, if no b -tagging, we have to consider all these direct backgrounds.

D. $e^- \gamma \rightarrow b \bar{t} \nu$

The contributing Feynman diagrams are shown in Fig. 3(a). This process was calculated in great details in Ref. [19]. The formulas for the matrix elements are also given in Appendix A. Its cross section is of order $0.02 - 0.1$ pb for the energy range of $\sqrt{s_{e^+e^-}} = 0.5 - 2$ TeV. The \bar{t} so produced will decay 100% into $\bar{b}W^-$ so that it can mimic the signal because there are, therefore, a W^- and $b\bar{b}$ pair plus missing energy due to the missing neutrino in the final state. However, the $b\bar{b}$ pair in this production does not likely form a sharp peak but a continuum background. The feasibility of detecting the $b\bar{b}$ pair resonance peak from the Higgs decay depends on whether the Higgs peak stands significantly (*e.g.*, $S/\sqrt{B} > 4$) above the continuum, and whether there are enough events under the Higgs-peak. We did an independent calculation, which agree with the results in Ref. [19], with full spin-correlation in the subsequent decay of $\bar{t} \rightarrow \bar{b}W^-$. Here we used a top-quark mass $m_t = 150$ GeV and a bottom-quark mass $m_b = 4.5$ GeV to illustrate.

The gluon parton inside the photon also contribute via electron-gluon scattering. Using the gluon distribution function described in Sec. II A, the contribution from the electron-gluon scattering can be as large as 50% at $\sqrt{s_{e^+e^-}} = 2$ TeV for DG, though it is only about 15% at 1 TeV, and negligible at 0.5 TeV. We will show the contribution from this “resolved” photon process in Fig. 4 and in our final results in the Tables, otherwise this contribution is left out in all the other figures.

E. $e^- \gamma \rightarrow t \bar{t} e^-$

The contributing Feynman diagrams are shown in Fig. 3(b), and the formulas for the helicity amplitudes are given in Appendix A. This is also a potential background when the t and \bar{t} decay into bW^+ and $\bar{b}W^-$ respectively, and only one of the W is detected. We

assume that the more energetic W is the one detected. In the final state there are therefore a W , $b\bar{b}$ pair plus missing energy due to the other undetected W and e^- . Similar to the previous background, the $b\bar{b}$ pair from $t\bar{t}e^-$ will not form a sharp resonance peak but a continuum. Here we included full spin-correlation in the subsequent decays of t and \bar{t} , and take $m_t = 150$ GeV. In this calculation we have neglected the contribution from “resolved” photon process, because it needs a rather high energy threshold for producing $t\bar{t}$ pair, where the gluon luminosity function drops to a small value. Other background arising from the QCD production of four jets are α_s^2 suppressed relative to the signal even before imposing the constraint of W or Z mass on the invariant mass of jet pairs, so these QCD backgrounds are negligible.

III. RESULTS

We use the following input parameters: $\alpha_w = 1/128$, $m_Z = 91.175$ GeV and $x_w = 0.23$, which on tree-level gives $m_W = 80.0057$ GeV. We show the total cross-sections for the signal and various backgrounds with $m_t = 150$ and $m_H = 100$ GeV for the center-of-mass energies $\sqrt{s_{e^+e^-}} = 0.5 - 2$ TeV in Fig. 4. We can see that the cross section of W^-Z is of order 0.1 – 1 pb for the energy range shown and the W^-W^+ production is of order 4 – 20 pb. On the other hand, the ZZ production is relatively negligible, and the signal WH production is only of order 0.01 – 0.2 pb. The other two backgrounds from $e^-\gamma \rightarrow \bar{t}b\nu$ and $t\bar{t}e^-$ are of more or less the same size as the WH signal. As mentioned above, the $p_T(VV)$ spectrum of the boson-pair can help to differentiate the signal and various backgrounds. In Fig. 5 we show the dependence of the differential cross section $d\sigma/dp_T(VV)$ on the transverse momentum of the boson-pair at $\sqrt{s} = 1$ and 2 TeV. In this figure, we did not include any branching fractions of the bosons. From this figure, we can choose an acceptance cut of

$$p_T(VV) > \begin{cases} 15 \text{ GeV} & \text{for } \sqrt{s} = 1 \text{ TeV} \\ 30 \text{ GeV} & \text{for } \sqrt{s} = 2 \text{ TeV}, \end{cases} \quad (7)$$

to reduce the WW background. We can also use the central electron vetoing [2,3], *i.e.*, rejecting events with electrons detected in the central region,

$$E(e) > 50 \text{ GeV} \quad \text{and} \quad |\cos \theta_e| < \cos(0.15), \quad (8)$$

to further reduce backgrounds that have e^- in the final state. Totally a factor of 10 reduction on WW background is achieved by combining the cuts of Eqs. (7) and (8), whereas it has almost no effect on the signal (see Table I).

Further reduction of backgrounds can be made possible by analyzing the direction of the outgoing boson-pair. We define the direction of the incoming e^- beam as the positive z -axis, and so the incoming photon beam as the negative z -axis. We select the W -boson in WZ production, W in WH , either W in WW , either Z in ZZ , W in $\bar{t}b\nu \rightarrow Wb\bar{b}\nu$, and the more energetic W in $t\bar{t}e^- \rightarrow b\bar{b}WWe^-$, as the boson V_1 ; and so the Z -boson in WZ , the H in WH , the other W in WW , the other Z in ZZ , the $b\bar{b}$ pair in $\bar{t}b\nu \rightarrow Wb\bar{b}\nu$ and the $b\bar{b}$ pair in $t\bar{t} \rightarrow b\bar{b}WWe^-$ as the boson V_2 . We then show the dependence of the differential cross-section on the cosine of the angle between the positive z -axis and the direction of the boson V_1 and V_2 in Fig. 6(a) and (b), respectively. We can see that the WW , ZZ , $b\bar{t}\nu$ and $t\bar{t}e^-$ backgrounds statistically have both bosons in the same hemisphere more often than in opposite ones, where the hemispheres are defined as the two half spaces separated by the plane that is perpendicular to the z -axis and contains the collision point. On the other hand, the events of WZ and WH tend to have the boson-pair coming out in opposite hemisphere. Therefore, we can reduce backgrounds by requiring the two bosons to come out in opposite hemisphere, *i.e.*,

$$\cos \theta_{V_1} \cos \theta_{V_2} < 0. \quad (9)$$

We also show the spectrum of $\cos \theta_{V_1} \cos \theta_{V_2}$ in Fig. 6(c). Actually, we could have been requiring $\cos \theta_{V_1} < 0$ and $\cos \theta_{V_2} > 0$, *i.e.*, V_1 going out in the “negative” ($\cos \theta < 0$) hemisphere and V_2 going out in the “positive” ($\cos \theta > 0$) hemisphere. We expect this additional acceptance cut could further reduce backgrounds by a large amount (see Fig. 6(a) and (b)).

However, there are uncertainties in determining which boson is V_1 or V_2 experimentally in the case of no b -tagging, and in the case of the backgrounds from ZZ and WW , plus the situation when m_H overlaps with m_Z or m_W then we could not determine which jet pair forms V_1 or V_2 . Therefore, we only employ the cut in Eq. (9) in the angular distributions of V_1 and V_2 so that we are safe from the above uncertainties. We can see from Table I that the cut of Eq. (9) actually cuts more on WW , ZZ , $t\bar{b}\nu$ and $t\bar{t}e^-$ than on the WH and WZ . We summarize in Table I the effectiveness of various combinations of cuts of Eq. (7), (8) and (9). After all these cuts, we can proceed to look at the invariant mass spectrum of the two jets that comes from the decay of the Higgs-boson or V_2 .

For the following we will consider two extreme cases: (a) with 100% efficient b -tagging and (b) without b -tagging. In the real experiment the situation will be in between these two extreme cases. For 100% efficient b -tagging the WWe^- background drops because we can require a $b\bar{b}$ pair in the final state and the decay of WW pair into $b\bar{b}$ pair is strongly suppressed by the Cabbibo mixing. Nevertheless, for the case of no b -tagging we have to consider all the backgrounds.

A. With 100% efficient b -tagging

Since the IMH predominately decays into $b\bar{b}$ pair (≈ 0.8 – 0.9) whereas the Z boson decay only 15% into $b\bar{b}$ (but about 70% into jets), therefore b -tagging can reduce the WZ and ZZ backgrounds by a factor of four to five. Note that $e\gamma \rightarrow e^-b\bar{b}Z$ is an order α_w suppressed. As mentioned above, the WW background is reducible with 100% b -tagging. The invariant mass $m(b\bar{b})$ spectra for the signal and various backgrounds are shown in Fig. 7 for $\sqrt{s_{e^+e^-}} = 1$ and 2 TeV, in which the branching fractions of $V_1 \rightarrow jj$ and $V_2 \rightarrow b\bar{b}$ are included. We use the $B(Z, W \rightarrow jj) \simeq 0.7$, $B(Z \rightarrow b\bar{b}) = 0.15$ and the $B(H \rightarrow b\bar{b})$ from Ref. [2]. As expected the $b\bar{b}$ pair from $t\bar{t}\nu$ and $t\bar{t}e^-$ productions form continuum spectra, while those from $WZ\nu$, ZZe^- and $WH\nu$ form discrete sharp peaks. These peaks, in collider experiments, actually spread out due to the resolution of the detector, though the Higgs width is very narrow

for the intermediate mass range that we are considering. We assume the peaks spread out uniformly over a range of ± 5 GeV about the central values (m_Z , m_W or m_H). We also assume that the Higgs peak is isolated if it is 10 GeV or more away from the Z -mass. In this case, the signal S is simply the cross section under the isolated peak, and the background B is the continuum background with $m(b\bar{b})$ falling in between $m_H \pm 5$ GeV. On the other hand, if $|m_H - m_Z| < 10$ GeV the Higgs and Z peaks are overlapping. In this case, we have to include the whole or part of the Z -peak into the background B . Naively, we can take a linear fraction of the Z -peak

$$\sigma(Z \text{ peak}) \times \frac{\max(0, 10 \text{ GeV} - |m_H - m_Z|)}{10 \text{ GeV}} \quad (10)$$

plus the continuum in between $m_H \pm 5$ GeV as the total background B .

In Fig. 7, the continuum backgrounds from $t\bar{b}\nu$ and $t\bar{t}e^-$ are rather flat, and far below the Higgs or Z peak. In this figure we show the Higgs-peak for $m_H = 100$ GeV, which is already slightly higher than the Z -peak. So we expect when the m_H goes down to 60 GeV (LEP limit) the Higgs peak will become higher because of the increase in both $\sigma(e\gamma \rightarrow WH\nu)$ and $B(H \rightarrow b\bar{b})$ as m_H decreases. Hence, we expect the discovery of the Higgs even with $m_H \simeq m_Z$ to be viable by employing the b -tagging. On the other hand, when m_H increases from 100 GeV the Higgs peak will decrease because of the decrease in both $\sigma(e\gamma \rightarrow WH\nu)$ and $B(H \rightarrow b\bar{b})$; especially after $m_H = 140$ GeV, the $B(H \rightarrow b\bar{b})$ drops sharply. Fortunately, at this range $m_H \gtrsim 100$ GeV the Higgs peak should be far away enough from the Z -peak, and the continuum backgrounds are far below. Therefore, the discovery of the Higgs depends only on the actual number of events under the Higgs peak. In Table II, we show the cross-sections in femtobarn for the signal S , various backgrounds, total background B and the corresponding significance S/\sqrt{B} of the signal, for various values of m_H from 60 – 160 GeV at $\sqrt{s_{e^+e^-}} = 1(2)$ TeV, with an assumed integrated luminosity of 10 fb^{-1} . We assume a signal of 6 or more events with a significance greater than 4 for the discovery of an isolated Higgs-peak; whereas in the case of overlapping Higgs-peak we require $S \geq 10$ with $S/\sqrt{B} > 6$ for discovery. With this criterion the Higgs boson can be discovered for $m_H = 60$ to 150 GeV

and marginally up to 160 GeV (see Table II) in $b\bar{b}$ decay mode, providing 100% efficient b -identification.

The signal for $m_H \simeq m_Z$ is slightly larger than the background, so with sufficient number of signal events the Higgs discovery at the Z -peak should be viable without knowing exactly the absolute normalization of the Z -peak. For those Higgs-masses away from the Z -mass the continuum background is so small that the actual number of signal events, which is the most important factor for Higgs discovery, is large enough up to $m_H = 150$ GeV. But as m_H increases from 150 GeV, the $B(H \rightarrow b\bar{b})$ goes down sharply from 18% to 3.7% at $m_H = 160$ GeV, and the number of signal events become marginal for discovery. Especially after $m_H = 160$ GeV, there are too few signal events for discovery.

So far we have assumed 100% acceptance and detection efficiencies for the jets decayed from the boson-pair. If we take into account the overall acceptance and detection efficiencies, say 25% overall, the number of signal and background events will decrease to 25%, and the significance S/\sqrt{B} will be halved. Even that we still have sufficient number of signal events and large enough S/\sqrt{B} to cover the whole range of $m_H = 60 - 150$ GeV, including $m_H \simeq m_Z$.

B. Without b -tagging

If without b -tagging there are several combinations of the four jets in the final state. One way to select the events is to pick out those that have two of the four jets reconstructed at the W -mass (Z -mass for ZZ , but it is negligible), then take the other two jets for considering the Higgs bosons. We assume this reconstruction can select the signal and the relevant background events very efficiently. We plot the spectrum of invariant mass of the third and fourth jets in Fig. 8. We can see that

- (i) the backgrounds from WZ , WW , after picking out the W (either Z for ZZ), form discrete peaks at either W or Z mass;

- (ii) the background from $b\bar{t}\nu \rightarrow b\bar{b}W^{-}\nu$, after picking out the W , the remaining $b\bar{b}$ can only form a continuum;
- (iii) for the $t\bar{t}e^{-} \rightarrow b\bar{b}WWe^{-}$, after picking out the more energetic W , we assume that we did not pick out the jet-pair from the other W . Therefore, the other two jets (from $b\bar{b}$) forms a continuum invariant-mass spectrum. Here we assumed this procedure is valid for our analysis, though experimentally we might pick out any two of the remaining four jets, or we might have picked out more than two parton-jets when they are close to one another;
- (iv) for the signal, after picking out the W , the $b\bar{b}$ will form a discrete peak at m_H .

The continuum backgrounds are rather flat, and far below the W , Z and Higgs peaks. So when the Higgs-peak is isolated it should be able to be discovered, provided that it has sufficient number of events under the peak. In this figure we show the Higgs peak for $m_H = 100$ GeV, and the Z -peak is about four times and the W -peak is eight times as high as the Higgs-peak. The Higgs peak, for the same reason mentioned in the last subsection, will become higher when m_H decreases, and smaller when m_H increases. Here we also have the cases whether the Higgs peak overlaps with the Z/W -peak or the Higgs peak is isolated. We take the same treatment as in the last subsection for the signal S and background B , but here we used the branching fractions of $V_1 \rightarrow jj$ and $V_2 \rightarrow jj$, and present the results in Table III. We assume a signal rate of 6 or more events with significance greater than 4 for the discovery of an isolated Higgs-peak; when the Higgs-peak overlaps with the W or Z -peak, absolute normalization of the W or Z - peak is important that we require more signal events ($\gtrsim 10$) with larger significance ($\gtrsim 6$) for the Higgs discovery in order to change the absolute normalization of the W or Z - peak by a significant amount. With this criterion, from Table III we should be able to discover the whole intermediate mass range of 60 to 150 GeV, and marginally upto 160 GeV.

The signal for $m_H \simeq m_W$ and m_Z is about $\frac{1}{6}$ and $\frac{1}{3}$ of the W - and Z -peak respectively (see Table III), but there are still sufficient number of signal events to affect the absolute

normalization of the W and Z peaks. When the Higgs peak is isolated from the W or Z peak, the Higgs discovery, which only depends on the actual number of signal events, should be viable up to about $m_H = 150$ GeV. However, as m_H increases from 150 GeV, the $B(H \rightarrow jj)$ drops very sharply, therefore the number of signal events becomes marginal for discovery, and after 160 GeV there are too few signal events.

Here we can also estimate the effect of overall acceptance and detection efficiencies of jets, say 25% overall. We should still have sufficient number of signal events and large enough significance to cover the whole range of 60 – 150 GeV, except for m_H right at m_W where the significance goes down below 6 to 3.8 (5.5) at $\sqrt{s} = 1(2)$ TeV, and for $m_H = m_Z$ where the significance goes down to 5.5 at $\sqrt{s} = 1$ TeV. The first exception should be cleaned up because $m_H \simeq m_W$ will be covered with ease at LEP II. The second exception is only slightly below our requirement of 6, so a slight increase in overall efficiency or \sqrt{s} can solve.

IV. CONCLUSIONS AND DISCUSSIONS

(i) We have done a signal-background analysis of the IMH search via the channel $e^- \gamma \rightarrow W^- H \nu \rightarrow (jj)(b\bar{b})\nu$ with and without considering b -identification, in a TeV $e^- \gamma$ collider, in which the photon beam is realized by the laser back-scattering method. The continuum backgrounds come from $e^- \gamma \rightarrow \bar{t}b\nu \rightarrow b\bar{b}\nu$ and $t\bar{t}e^- \rightarrow b\bar{b}WWe^-$, while the discrete backgrounds come from $e^- \gamma \rightarrow W^- Z \nu$, WWe^- and ZZe^- . We showed the results at both 1 and 2 TeV e^+e^- machines, between which the $WH\nu$ production is large enough for IMH discovery. However, at 0.5 TeV the $WH\nu$ production is too small for any realistic Higgs search.

(ii) With 100% b -identification the discovery of Higgs for the whole range of $m_H = 60 - 150$ GeV (marginally upto 160 GeV) should be viable at both $\sqrt{s_{e^+e^-}} = 1$ and 2 TeV. With $m_H \simeq m_Z$, since the signal is slightly larger than the background, the exact absolute normalization of the Z -peak is not important.

(iii) Without b -identification the whole range of $m_H = 60 - 150$ GeV (marginally upto

160 GeV) should be covered at both energies. With $m_H \simeq m_W$ or m_Z the background is several times larger, therefore absolute normalization of the W and Z peaks is important. Fortunately, there are sufficient number of signal events to affect the absolute normalization.

(iv) All the cross-sections in the Tables are assuming that the jets are recognized with 100% efficiency. We also tried to estimate the effect of 25% overall acceptance and detection efficiencies. In this case, the signal and background events go down to 25%, and the significance S/\sqrt{B} is halved. As mentioned in previous section, even with this overall efficiencies, the whole range of $m_H = 60 - 150$ GeV should be covered for both cases: with and without considering b -identification.

(v) In the real collider experiment, the b -identification efficiency will be somewhere between our two extreme cases. Therefore, we expect the Higgs discovery should be viable for the whole range of $m_H = 60 - 150$ GeV between $\sqrt{s_{e^+e^-}} = 1$ and 2 TeV inclusively, provided that the absolute normalization of the W and Z peak is known to a certain accuracy. At $\sqrt{s_{e^+e^-}} = 2$ TeV, the search for the IMH is actually doing a little better, though not much, than that at 1 TeV because it has about twice the signal, but also twice the discrete backgrounds, and slightly less continuum background.

(v) In estimating the continuum background we take the invariant-mass $m(b\bar{b})$ or $m(j\bar{j})$ in the interval $m_H \pm 5$ GeV. Due to limitations of the detector we may not be able to achieve this resolution, then we have to relax this stringent requirement by some extent. For example, if we take $m_H \pm 10$ GeV, which is quite conservative, the background coming from the continuum increases by a factor of 2, because the continuum background is rather flat (see Figs. 7 and 8). In this case, the significance of the isolated Higgs-signal is reduced by $\sqrt{2}$. From Tables II and III we can see that even though the significance of the signal (away from the W or Z -peak) is reduced by such factor, it is still large enough for Higgs discovery.

(vi) In calculating the contribution from the resolved photon processes, we used the DG parameterization [17] for the photon structure function. DG has a relatively soft gluon spectrum. If we choose LAC3 [20] parameterization, which has a relatively harder gluon spectrum, the contribution from resolved photon process is expected to increase by a factor

of 2 – 3. Even that the continuum is still far below the Higgs-signal peak (see Figs. 7 and 8), so this will not affect our conclusions.

(vii) the effective $e\gamma$ luminosity might be less than the original electron-positron luminosity [15]. This fact will reduce our signal and backgrounds by the same amount, but will reduce the significance of the signal, thus making the discovery of Higgs boson more difficult. However, this channel is still useful because in the future there are likely improvements in the machine design that can optimize the effective luminosity.

ACKNOWLEDGMENTS

This work was supported by the U. S. Department of Energy, Division of High Energy Physics, under Grant DE-FG02-91-ER40684.

APPENDIX A

In this appendix we present the matrix elements for processes $e^- \gamma \rightarrow W^- H \nu$, $W^- Z \nu$, $W^- W^+ e^-$, ZZe^- , $\bar{t} b \nu$ and $t \bar{t} e^-$, from which explicit helicity amplitudes can be directly computed. To start with, we introduce some general notation:

$$g_a^W(f) = -g_b^W(f) = \frac{g}{2\sqrt{2}}, \quad (\text{A1})$$

$$g_a^Z(f) = g_Z \left(\frac{T_{3f}}{2} - Q_f x_w \right), \quad (\text{A2})$$

$$g_b^Z(f) = -g_Z \frac{T_{3f}}{2}, \quad (\text{A3})$$

$$g_a^\gamma(f) = e Q_f, \quad (\text{A4})$$

$$g_b^\gamma(f) = 0, \quad (\text{A5})$$

$$g^V(f) = g_a^V(f) + g_b^V(f) \gamma^5 \quad (V = \gamma, W, Z), \quad (\text{A6})$$

$$D^X(k) = \frac{1}{k^2 - M_X^2 + i\Gamma_X(k^2)m_X}, \quad \Gamma_X(k^2) = \Gamma_X \theta(k^2) \\ (\text{with } X = \gamma, W, Z, H), \quad (\text{A7})$$

$$P_V^{\alpha\beta}(k) = \left[g^{\alpha\beta} + \frac{(1-\xi)k^\alpha k^\beta}{\xi k^2 - m_V^2} \right] D^V(k), \quad (\text{A8})$$

$$\Gamma^\alpha(k_1, k_2; \epsilon_1, \epsilon_2) = (k_1 - k_2)^\alpha \epsilon_1 \cdot \epsilon_2 + (2k_2 + k_1) \cdot \epsilon_1 \epsilon_2^\alpha - (2k_1 + k_2) \cdot \epsilon_2 \epsilon_1^\alpha, \quad (\text{A9})$$

$$g_{VWW} = \begin{cases} e \cot \theta_w & \text{for } V = Z \\ e & \text{for } V = \gamma. \end{cases} \quad (\text{A10})$$

Here Q_f and T_{3f} are the electric charge (in units of the positron charge) and the third component of weak isospin of the fermion f , g is the SU(2) gauge coupling, and $g_Z = g/\cos\theta_w$, $x_w = \sin^2\theta_w$, with θ_w being the weak mixing angle in the Standard Model. Dots between 4-vectors denote scalar products and $g_{\alpha\beta}$ is the Minkowskian metric tensor with $g_{00} = -g_{11} = -g_{22} = -g_{33} = 1$; ξ is a gauge-fixing parameter.

In Figs. 1 and 2, the momentum-labels p_i denote the momenta flowing along the corresponding fermion lines in the direction of the arrows. We shall denote the associated spinors by the symbols $u(p_i)$ and $\bar{u}(p_i)$ for the incoming and outgoing arrows, which is usual for

the annihilation and creation of fermions, respectively. In Fig. 3 there is also creation of anti-fermion (corresponding to an incoming arrow labeled by negative momentum $-p_i$), we shall denote its associated spinor by $v(p_i)$.

1. $e^- \gamma \rightarrow W^- H \nu$

The contributing Feynman diagrams for $e^-(p_1)\gamma(p_2) \rightarrow W^-(k_1)H(k_2)\nu(q_1)$ are shown in Fig. 1. We define a shorthand notation

$$J_1^\mu = \bar{u}(q_1)\gamma^\mu g^W(e)u(p_1) \times D^W(p_1 - q_1), \quad (\text{A11})$$

then the helicity amplitudes are given by

$$\mathcal{M}^{(a)} = g^2 m_W \sin \theta_w P_W^{\alpha\beta}(p_2 - k_1) \Gamma_\alpha(-k_1, p_2; \epsilon(k_1), \epsilon(p_2)) J_{1\beta}, \quad (\text{A12})$$

$$\mathcal{M}^{(b)} = -g^2 m_W \sin \theta_w \epsilon(p_2) \cdot \epsilon(k_1) k_2 \cdot J_1 \frac{\xi}{\xi(p_2 - k_1)^2 - m_W^2}, \quad (\text{A13})$$

$$\mathcal{M}^{(c)} = g^2 m_W \sin \theta_w P_W^{\alpha\beta}(k_1 + k_2) \Gamma_\alpha(p_2, p_1 - q_1; \epsilon(p_2), J_1) \epsilon_\beta(k_1), \quad (\text{A14})$$

$$\mathcal{M}^{(d)} = g^2 m_W \sin \theta_w \epsilon(p_2) \cdot J_1 k_2 \cdot \epsilon(k_1) \frac{\xi}{\xi(k_1 + k_2)^2 - m_W^2}, \quad (\text{A15})$$

$$\begin{aligned} \mathcal{M}^{(e)} &= -g m_W P_W^{\alpha\beta}(k_1 + k_2) \epsilon_\alpha(k_1) \\ &\times \bar{u}(q_1) \gamma_\beta g^W(e) \frac{\not{p}_1 + \not{p}_2 + m_e}{(p_1 + p_2)^2 - m_e^2} \not{\epsilon}(p_2) g^\gamma(e) u(p_1), \end{aligned} \quad (\text{A16})$$

2. $e^- \gamma \rightarrow W^- Z \nu$

The contributing Feynman diagrams for $e^-(p_1)\gamma(p_2) \rightarrow W^-(k_1)Z(k_2)\nu(q_1)$ are given in Fig. 2(a). We define a shorthand notation

$$J_1^\mu = \bar{u}(q_1)\gamma^\mu g^W(e)u(p_1) \times D^W(p_1 - q_1), \quad (\text{A17})$$

then the helicity amplitudes are given by

$$\begin{aligned} \mathcal{M}^{(a)} &= -g_{ZW} g_{WW} \Gamma_\alpha(-k_1, p_2; \epsilon(k_1), \epsilon(p_2)) P_W^{\alpha\beta}(p_2 - k_1) \\ &\times \Gamma_\beta(-k_2, p_1 - q_1; \epsilon(k_2), J_1), \end{aligned} \quad (\text{A18})$$

$$\begin{aligned} \mathcal{M}^{(b)} &= -g_{ZWW}g_{\gamma WW}\Gamma_\alpha(k_2, k_1; \epsilon(k_2), \epsilon(k_1))P_W^{\alpha\beta}(k_1 + k_2) \\ &\quad \times \Gamma_\beta(p_2, p_1 - q_1; \epsilon(p_2), J_1), \end{aligned} \quad (\text{A19})$$

$$\begin{aligned} \mathcal{M}^{(c)} &= g_{ZWW}g_{\gamma WW}[2\epsilon(p_2) \cdot \epsilon(k_2)\epsilon(k_1) \cdot J_1 - \epsilon(p_2) \cdot J_1\epsilon(k_1) \cdot \epsilon(k_2) \\ &\quad - \epsilon(p_2) \cdot \epsilon(k_1)\epsilon(k_2) \cdot J_1], \end{aligned} \quad (\text{A20})$$

$$\begin{aligned} \mathcal{M}^{(d,e)} &= g_{\gamma WW}\Gamma_\alpha(-k_1, p_2; \epsilon(k_1), \epsilon(p_2))P_W^{\alpha\beta}(p_2 - k_1) \\ &\quad \times \left[\bar{u}(q_1)\gamma_\beta g^W(e)\frac{\not{p}_1 - \not{k}_2 + m_e}{(p_1 - k_2)^2 - m_e^2}\not{\epsilon}(k_2)g^Z(e)u(p_1) \right. \\ &\quad \left. + \bar{u}(q_1)\not{\epsilon}(k_2)g^Z(\nu)\frac{\not{q}_1 + \not{k}_2}{(q_1 + k_2)^2}\gamma_\beta g^W(e)u(p_1) \right], \end{aligned} \quad (\text{A21})$$

$$\begin{aligned} \mathcal{M}^{(f)} &= g_{ZWW}\Gamma_\alpha(k_2, k_1; \epsilon(k_2), \epsilon(k_1))P_W^{\alpha\beta}(k_1 + k_2) \\ &\quad \times \bar{u}(q_1)\gamma_\beta g^W(e)\frac{\not{p}_1 + \not{p}_2 + m_e}{(p_1 + p_2)^2 - m_e^2}\not{\epsilon}(p_2)g^\gamma(e)u(p_1), \end{aligned} \quad (\text{A22})$$

$$\begin{aligned} \mathcal{M}^{(g)} &= -\bar{u}(q_1)\not{\epsilon}(k_1)g^W(e)\frac{\not{q}_1 + \not{k}_1 + m_e}{(q_1 + k_1)^2 - m_e^2}\not{\epsilon}(k_2)g^Z(e)\frac{\not{p}_1 + \not{p}_2 + m_e}{(p_1 + p_2)^2 - m_e^2} \\ &\quad \not{\epsilon}(p_2)g^\gamma(e)u(p_1), \end{aligned} \quad (\text{A23})$$

$$\begin{aligned} \mathcal{M}^{(h)} &= -\bar{u}(q_1)\not{\epsilon}(k_1)g^W(e)\frac{\not{q}_1 + \not{k}_1 + m_e}{(q_1 + k_1)^2 - m_e^2}\not{\epsilon}(p_2)g^\gamma(e)\frac{\not{p}_1 - \not{k}_2 + m_e}{(p_1 - k_2)^2 - m_e^2} \\ &\quad \not{\epsilon}(k_2)g^Z(e)u(p_1), \end{aligned} \quad (\text{A24})$$

$$\begin{aligned} \mathcal{M}^{(i)} &= -\bar{u}(q_1)\not{\epsilon}(k_2)g^Z(\nu)\frac{\not{q}_1 + \not{k}_2}{(q_1 + k_2)^2}\not{\epsilon}(k_1)g^W(e)\frac{\not{p}_1 + \not{p}_2 + m_e}{(p_1 + p_2)^2 - m_e^2} \\ &\quad \not{\epsilon}(p_2)g^\gamma(e)u(p_1), \end{aligned} \quad (\text{A25})$$

$$\mathcal{M}^{(j)} = -g^2m_W^2x_w \tan\theta_w \frac{\xi}{\xi(p_2 - k_1)^2 - m_W^2} \epsilon(k_1) \cdot \epsilon(p_2) \epsilon(k_2) \cdot J_1 \quad (\text{A26})$$

$$\mathcal{M}^{(k)} = -g^2m_W^2x_w \tan\theta_w \frac{\xi}{\xi(k_1 + k_2)^2 - m_W^2} \epsilon(k_1) \cdot \epsilon(k_2) \epsilon(p_2) \cdot J_1. \quad (\text{A27})$$

3. $e^- \gamma \rightarrow W^- W^+ e^-$

The contributing Feynman diagrams for the process $e^-(p_1)\gamma(p_2) \rightarrow W^-(k_1)W^+(k_2)e^-(q_1)$ are shown in Fig. 2(b). We can also define a shorthand notation

$$J_V^\mu = \bar{u}(q_1)\gamma^\mu g^V(e)u(p_1) \times D^V(p_1 - q_1), \quad \text{where } V = \gamma, Z \quad (\text{A28})$$

then the helicity amplitudes are given by

$$\begin{aligned} \mathcal{M}^{(a)} = & \sum_{V=\gamma,Z} -g_{VWW} g_{\gamma WW} P_W^{\alpha\beta} (p_2 - k_2) \\ & \times \Gamma_\alpha(-k_1, p_1 - q_1; \epsilon(k_1), J_V) \Gamma_\beta(p_2, -k_2; \epsilon(p_2), \epsilon(k_2)), \end{aligned} \quad (\text{A29})$$

$$\begin{aligned} \mathcal{M}^{(b)} = & \sum_{V=\gamma,Z} -g_{VWW} g_{\gamma WW} P_W^{\alpha\beta} (p_2 - k_1) \\ & \times \Gamma_\alpha(p_1 - q_1, -k_2; J_V, \epsilon(k_2)) \Gamma_\beta(-k_1, p_2; \epsilon(k_1), \epsilon(p_2)), \end{aligned} \quad (\text{A30})$$

$$\begin{aligned} \mathcal{M}^{(c)} = & \sum_{V=\gamma,Z} g_{VWW} g_{\gamma WW} [2\epsilon(k_1) \cdot \epsilon(k_2) \epsilon(p_2) \cdot J_V \\ & - \epsilon(k_1) \cdot J_V \epsilon(k_2) \cdot \epsilon(p_2) - \epsilon(k_2) \cdot J_V \epsilon(k_1) \cdot \epsilon(p_2)], \end{aligned} \quad (\text{A31})$$

$$\begin{aligned} \mathcal{M}^{(d)} = & -\bar{u}(q_1) \not{\epsilon}(k_2) g^W(e) \frac{\not{q}_1 + \not{k}_2}{(q_1 + k_2)^2} \not{\epsilon}(k_1) g^W(e) \frac{\not{p}_1 + \not{p}_2 + m_e}{(p_1 + p_2)^2 - m_e^2} \\ & \not{\epsilon}(p_2) g^\gamma(e) u(p_1), \end{aligned} \quad (\text{A32})$$

$$\begin{aligned} \mathcal{M}^{(e)} = & -\bar{u}(q_1) \not{\epsilon}(p_2) g^\gamma(e) \frac{\not{q}_1 - \not{p}_2 + m_e}{(q_1 - p_2)^2 - m_e^2} \not{\epsilon}(k_2) g^W(e) \frac{\not{p}_1 - \not{k}_1}{(p_1 - k_1)^2} \\ & \not{\epsilon}(k_1) g^W(e) u(p_1), \end{aligned} \quad (\text{A33})$$

$$\begin{aligned} \mathcal{M}^{(f)} = & \sum_{V=\gamma,Z} g_{VWW} D^V(k_1 + k_2) \Gamma_\alpha(k_1, k_2; \epsilon(k_1), \epsilon(k_2)) \\ & \times \bar{u}(q_1) \gamma^\alpha g^V(e) \frac{\not{p}_1 + \not{p}_2 + m_e}{(p_1 + p_2)^2 - m_e^2} \not{\epsilon}(p_2) g^\gamma(e) u(p_1), \end{aligned} \quad (\text{A34})$$

$$\begin{aligned} \mathcal{M}^{(g)} = & \sum_{V=\gamma,Z} g_{VWW} D^V(k_1 + k_2) \Gamma_\alpha(k_1, k_2; \epsilon(k_1), \epsilon(k_2)) \\ & \times \bar{u}(q_1) \not{\epsilon}(p_2) g^\gamma(e) \frac{\not{q}_1 - \not{p}_2 + m_e}{(q_1 - p_2)^2 - m_e^2} \gamma^\alpha g^V(e) u(p_1), \end{aligned} \quad (\text{A35})$$

$$\begin{aligned} \mathcal{M}^{(h)} = & g_{\gamma WW} P_W^{\alpha\beta} (p_2 - k_2) \Gamma_\alpha(p_2, -k_2; \epsilon(p_2), \epsilon(k_2)) \\ & \times \bar{u}(q_1) \gamma_\beta g^W(e) \frac{\not{p}_1 - \not{k}_1}{(p_1 - k_1)^2} \not{\epsilon}(k_1) g^W(e) u(p_1), \end{aligned} \quad (\text{A36})$$

$$\begin{aligned} \mathcal{M}^{(i)} = & g_{\gamma WW} P_W^{\alpha\beta} (p_2 - k_1) \Gamma_\alpha(-k_1, p_2; \epsilon(k_1), \epsilon(p_2)) \\ & \times \bar{u}(q_1) \not{\epsilon}(k_2) g^W(e) \frac{\not{q}_1 + \not{k}_2}{(q_1 + k_2)^2} \gamma_\beta g^W(e) u(p_1), \end{aligned} \quad (\text{A37})$$

$$\begin{aligned} \mathcal{M}^{(j)} = & \sum_{V=\gamma,Z} g^2 m_W^2 x_w \frac{\xi}{\xi(p_2 - k_2)^2 - m_W^2} \epsilon(p_2) \cdot \epsilon(k_2) \epsilon(k_1) \cdot J_V \\ & \times \begin{cases} -\tan \theta_w & \text{for } V = Z \\ 1 & \text{for } V = \gamma \end{cases}, \end{aligned} \quad (\text{A38})$$

$$\mathcal{M}^{(k)} = \sum_{V=\gamma,Z} g^2 m_W^2 x_w \frac{\xi}{\xi(p_2 - k_1)^2 - m_W^2} \epsilon(p_2) \cdot \epsilon(k_1) \epsilon(k_2) \cdot J_V$$

$$\times \begin{cases} -\tan\theta_w & \text{for } V = Z \\ 1 & \text{for } V = \gamma \end{cases}. \quad (\text{A39})$$

4. $e^- \gamma \rightarrow ZZ e^-$

The contributing Feynman diagrams for the process $e^-(p_1)\gamma(p_2) \rightarrow Z(k_1)Z(k_2)e^-(q_1)$ are the same as the diagram (e) in Fig. 2(b) with the W -bosons replaced by Z -bosons plus all possible permutations. Totally it has six contributing Feynman diagrams. They are given by

$$\begin{aligned} \mathcal{M}^{(a)} = & -\bar{u}(q_1)\not{\epsilon}(k_1)g^Z(e)\frac{\not{q}_1 + \not{k}_1 + m_e}{(q_1 + k_1)^2 - m_e^2}\not{\epsilon}(k_2)g^Z(e)\frac{\not{p}_1 + \not{p}_2 + m_e}{(p_1 + p_2)^2 - m_e^2} \\ & \not{\epsilon}(p_2)g^\gamma(e)u(p_1), \end{aligned} \quad (\text{A40})$$

$$\begin{aligned} \mathcal{M}^{(b)} = & -\bar{u}(q_1)\not{\epsilon}(k_1)g^Z(e)\frac{\not{q}_1 + \not{k}_1 + m_e}{(q_1 + k_1)^2 - m_e^2}\not{\epsilon}(p_2)g^\gamma(e)\frac{\not{p}_1 - \not{k}_2 + m_e}{(p_1 - k_2)^2 - m_e^2} \\ & \not{\epsilon}(k_2)g^Z(e)u(p_1), \end{aligned} \quad (\text{A41})$$

$$\begin{aligned} \mathcal{M}^{(c)} = & -\bar{u}(q_1)\not{\epsilon}(p_2)g^\gamma(e)\frac{\not{q}_1 - \not{p}_2 + m_e}{(q_1 - p_2)^2 - m_e^2}\not{\epsilon}(k_1)g^Z(e)\frac{\not{p}_1 - \not{k}_2 + m_e}{(p_1 - k_2)^2 - m_e^2} \\ & \not{\epsilon}(k_2)g^Z(e)u(p_1), \end{aligned} \quad (\text{A42})$$

plus those terms with $(k_1 \leftrightarrow k_2)$.

5. $e^- \gamma \rightarrow \bar{t}b\nu$

The contributing Feynman diagrams for $e^-(p_1)\gamma(p_2) \rightarrow \bar{t}(k_1)b(k_2)\nu(q_1)$ are shown in Fig. 3(a). We define the following shorthand notation:

$$J_1^\mu = \bar{u}(q_1)\gamma^\mu g^W(e)u(p_1) \times D^W(p_1 - q_1), \quad (\text{A43})$$

then the helicity amplitudes are given by

$$\mathcal{M}^{(a)} = \bar{u}(k_2)\not{\epsilon}(p_2)g^\gamma(b)\frac{\not{k}_2 - \not{p}_2 + m_b}{(k_2 - p_2)^2 - m_b^2}J_1 g^W(t)v(k_1), \quad (\text{A44})$$

$$\mathcal{M}^{(b)} = \bar{u}(k_2)J_1 g^W(t)\frac{\not{p}_2 - \not{k}_1 + m_t}{(p_2 - k_1)^2 - m_t^2}\not{\epsilon}(p_2)g^\gamma(t)v(k_1), \quad (\text{A45})$$

$$\begin{aligned} \mathcal{M}^{(c)} &= -g \sin \theta_w P_W^{\alpha\beta}(k_1 + k_2) \bar{u}(k_2) \gamma_\alpha g^W(t) v(k_1) \\ &\quad \times \Gamma_\beta(p_2, p_1 - q_1; \epsilon(p_2), J_1), \end{aligned} \quad (\text{A46})$$

$$\begin{aligned} \mathcal{M}^{(d)} &= \frac{g^2}{2\sqrt{2}} \sin \theta_w \epsilon(p_2) \cdot J_1 \frac{\xi}{\xi(k_1 + k_2)^2 - m_W^2} \\ &\quad \times \bar{u}(k_2) \left[(m_t - m_b) + (m_t + m_b) \gamma^5 \right] v(k_1), \end{aligned} \quad (\text{A47})$$

$$\begin{aligned} \mathcal{M}^{(e)} &= \bar{u}(q_1) \gamma_\alpha g^W(e) \frac{\not{p}_1 + \not{p}_2 + m_e}{(p_1 + p_2)^2 - m_e^2} \not{\epsilon}(p_2) g^\gamma(e) u(p_1) \\ &\quad \times P_W^{\alpha\beta}(k_1 + k_2) \bar{u}(k_2) \gamma_\beta g^W(t) v(k_1). \end{aligned} \quad (\text{A48})$$

The diagrams for the “resolved” photon process $e^- g \rightarrow \bar{t} b \nu$ are the same as diagrams (a) and (b) in Fig. 3(a), with the photon replaced by the gluon. The helicity amplitudes are the same except with the coupling g^γ replaced by g_s , and a different color factor. The color factor to multiply the matrix element squared is 3 and 1/2 for the $e\gamma$ and the resolved process, respectively.

6. $e^- \gamma \rightarrow t \bar{t} e^-$

The contributing Feynman diagrams for $e^-(p_1) \gamma(p_2) \rightarrow \bar{t}(k_1) t(k_2) e^-(q_1)$ are shown in Fig. 3(b). We also define the shorthand notations:

$$\begin{aligned} J_{V_e}^\mu &= \bar{u}(q_1) \gamma^\mu g^V(e) u(p_1) \times D^V(p_1 - q_1), \\ J_{V_t}^\mu &= \bar{u}(k_2) \gamma^\mu g^V(t) v(k_1) \times D^V(k_1 + k_2), \end{aligned} \quad (\text{A49})$$

then the helicity amplitudes are given by

$$\mathcal{M}^{(a)} = \sum_{V=\gamma,Z} \bar{u}(k_2) \not{\epsilon}(p_2) g^\gamma(t) \frac{\not{k}_2 - \not{p}_2 + m_t}{(k_2 - p_2)^2 - m_t^2} J_{V_e} g^V(t) v(k_1), \quad (\text{A50})$$

$$\mathcal{M}^{(b)} = \sum_{V=\gamma,Z} \bar{u}(k_2) J_{V_e} g^V(t) \frac{\not{p}_2 - \not{k}_1 + m_t}{(p_2 - k_1)^2 - m_t^2} \not{\epsilon}(p_2) g^\gamma(t) v(k_1), \quad (\text{A51})$$

$$\mathcal{M}^{(c)} = \sum_{V=\gamma,Z} \bar{u}(q_1) J_{V_t} g^V(e) \frac{\not{p}_1 + \not{p}_2 + m_e}{(p_1 + p_2)^2 - m_e^2} \not{\epsilon}(p_2) g^\gamma(e) u(p_1), \quad (\text{A52})$$

$$\mathcal{M}^{(d)} = \sum_{V=\gamma,Z} \bar{u}(q_1) \not{\epsilon}(p_2) g^\gamma(e) \frac{\not{q}_1 - \not{p}_2 + m_e}{(q_1 - p_2)^2 - m_e^2} J_{V_t} g^V(e) u(p_1). \quad (\text{A53})$$

The color factor to multiply the matrix element squared is 3 for this process.

These matrix elements are to be squared, summed over polarizations and spins of the final state gauge-bosons and fermions respectively, and then averaged over the polarizations of the incoming photon and spins of the initial state electron. Then the cross section σ is obtained by folding the subprocess cross-section $\hat{\sigma}$ in with the photon luminosity function as

$$\sigma(s) = \int_{M_{\text{final}}/s}^{x_{\text{max}}} dx F_{\gamma/e}(x) \hat{\sigma}(\hat{s} = xs), \quad (\text{A54})$$

where

$$\begin{aligned} \hat{\sigma}(\hat{s}) = & \frac{1}{2(\hat{s}-m_e^2)} \int \frac{d^3 k_1}{(2\pi)^3 k_1^0} \frac{d^3 k_2}{(2\pi)^3 k_2^0} \frac{d^3 q_1}{(2\pi)^3 q_1^0} \\ & \times (2\pi)^4 \delta^{(4)}(p_1 + p_2 - k_1 - k_2 - q_1) \sum |\mathcal{M}|^2 \end{aligned} \quad (\text{A55})$$

and M_{final} is the sum of the masses of the final state particles.

REFERENCES

- [1] V. Barger, K. Cheung, T. Han, D. Zeppenfeld and J. Ohnemus, Phys. Rev. **D44**, 1426 (1991); V. Barger, T. Han and R. N. J. Phillips, Phys. Lett. **B200**, 193 (1988); U. Baur and E. W. N. Glover, Phys. Rev. **D44**, 99 (1991).
- [2] V. Barger, K. Cheung, B. Kniehl and R. J. N. Phillips, Phys. Rev. **D46**, 3725 (1992).
- [3] K. Hagiwara, J. Kanzaki and H. Murayama, Durham University Report DTP-91-18 (1991), unpublished.
- [4] E. Gross and P. Yepes, Int. J. Mod. Phys. **A8**, 407 (1993).
- [5] GEM Letter of Intent, contact persons: B. Barish and W. Willis, Nov. 31, 1991.
- [6] R. Kleiss, Z. Kunszt and W. J. Stirling, Phys. Lett **B253**, 269 (1991).
- [7] W. Marciano and F. Paige, Phys. Rev. Lett **66**, 2433 (1991); J. F. Gunion, Phys. Lett. **B261**, 510 (1991); Z. Kunszt, Z. Trócsányi and W. J. Stirling, Phys. Lett. **B271**, 247 (1991).
- [8] P. Janot, Osray preprints LAL-92-27.
- [9] D. Borden, D. Bauer and D. Caldwell, SLAC preprint, SLAC-PUB-5715, (1992).
- [10] F. Richard, talk given at International meeting of EE500 working groups at Annecy, June 10-11, 1991, LAL 91-62.
- [11] D. Bowser-Chao and K. Cheung, Northwestern preprint, NUHEP-TH-92-29, (1992).
- [12] K. Cheung, Northwestern preprint, NUHEP-TH-92-21 (1992), to appear in Phys. Rev. D; E. Boos, *et al.*, MPI preprint MPI-Ph/92-48.
- [13] E. Boos, *et al.*, Phys. Lett. **B273**, 173 (1991).
- [14] K. Hagiwara, I. Watanabe, and P. Zerwas, Phys. Lett. **B278**, 187 (1992).

- [15] V. Telnov, Nucl. Instr. & Methods **A294**, 72 (1990); I. Ginzburg, G. Kotkin, V. Serbo and V. Telnov, Nucl. Instr. & Methods **205**, 47 (1983); *idem* **219**, 5 (1984).
- [16] E. Witten, Nucl. Phys. **B120**,189 (1977).
- [17] M. Drees and K. Grassie, Z. Phys. **C28**, 451 (1985).
- [18] K. Cheung, Northwestern preprint NUHEP-TH-92-24 (1992).
- [19] G. Jikia, Nucl. Phys. **B374**, 83 (1992).
- [20] H. Abramowicz, K. Charchula and A. Levy, Phys. Lett. **B269**, 458 (1991).

TABLES

TABLE I. Table showing the effectiveness of various combinations of the cuts in Eqs. (7), (8) and (9) for $\sqrt{s_{e^+e^-}} = 1(2)$ TeV, with $m_t = 150$ and $m_H = 100$ GeV. The cross-sections are given in the unit of fb. No branching fractions of the bosons are included. The numbers in the parenthesis are for $\sqrt{s_{e^+e^-}} = 2$ TeV.

Combinations	WH	WZ	WW	ZZ	$e^-\gamma \rightarrow b\bar{t}\nu$	$e^-g \rightarrow b\bar{t}\nu$	$t\bar{t}e^-$
(a) No cuts	79 (200)	390 (970)	10400 (19500)	10 (6.8)	55 (91)	8.1 (43)	83 (160)
(b) Eq. (7)	73 (160)	380 (930)	1960 (2960)	2.7 (1.9)	52 (79)	7.2 (31)	79 (150)
(c) Eqs. (7) and (8)	73 (160)	380 (930)	900 (1800)	0.54 (0.24)	52 (79)	7.2 (31)	66 (130)
(d) Eqs. (7), (8) and (9)	55 (110)	250 (560)	510 (1000)	0.19 (0.083)	20 (22)	2.4 (7.7)	22 (22)

TABLE II. Cross-sections (fb) for the signal and various backgrounds, total background B , and the significance S/\sqrt{B} (integrated luminosity=10 fb⁻¹) of the signal for $m_H = 60 - 160$ GeV at $\sqrt{s_{e^+e^-}} = 1(2)$ TeV. Here the acceptance cuts are Eqs. (7), (8) and (9). The discrete backgrounds are calculated using Eq. (10) and the continuum backgrounds are with $m(b\bar{b})$ in between $m_H \pm 5$ GeV. Also we assume 100% b -tagging, $m_t = 150$ GeV, and the branching fractions of the $V_1 \rightarrow jj$ and $V_2 \rightarrow b\bar{b}$ are included.

m_H	signal	discrete backgrounds			continuum backgrounds			total B	S/\sqrt{B} 10 fb ⁻¹
	WH	WZ	WW	ZZ	$\bar{t}b\nu$	$e^-g \rightarrow \bar{t}b\nu$	$t\bar{t}e^-$		
60	40 (75)	0 (0)	0 (0)	0 (0)	0.56 (0.34)	0.18 (0.40)	0.89 (0.67)	1.6 (1.4)	99 (200)
70	36 (72)	0 (0)	0 (0)	0 (0)	0.59 (0.39)	0.12 (0.37)	0.90 (0.74)	1.6 (1.5)	90 (186)
80	35 (69)	0 (0)	0 (0)	0 (0)	0.58 (0.41)	0.10 (0.32)	0.88 (0.72)	1.6 (1.5)	89 (181)
90	33 (67)	23 (52)	0 (0)	0.035 (0.015)	0.56 (0.41)	0.083 (0.28)	0.83 (0.70)	25 (53)	21 (29)
100	31 (64)	3.0 (6.9)	0 (0)	0.0047 (0.0020)	0.52 (0.41)	0.074 (0.24)	0.78 (0.66)	4.4 (8.2)	47 (71)
110	28 (59)	0 (0)	0 (0)	0 (0)	0.52 (0.41)	0.055 (0.21)	0.74 (0.62)	1.3 (1.2)	77 (168)
120	24 (50.5)	0 (0)	0 (0)	0 (0)	0.50 (0.41)	0.045 (0.18)	0.70 (0.58)	1.2 (1.2)	68 (148)
130	17.5 (38)	0 (0)	0 (0)	0 (0)	0.48 (0.41)	0.040 (0.15)	0.64 (0.53)	1.2 (1.1)	51 (115)
140	11 (24.5)	0 (0)	0 (0)	0 (0)	0.47 (0.41)	0.034 (0.13)	0.61 (0.51)	1.1 (1.1)	33 (76)
150	5.3 (12)	0 (0)	0 (0)	0 (0)	0.46 (0.40)	0.028 (0.12)	0.55 (0.47)	1.0 (0.99)	16 (38)
160	1.0 (2.4)	0 (0)	0 (0)	0 (0)	0.45 (0.39)	0.021 (0.10)	0.51 (0.46)	0.98 (0.96)	3.2 (7.8)

TABLE III. Cross-sections (fb) for the signal and various backgrounds, total background B , and the significance S/\sqrt{B} (integrated luminosity=10 fb⁻¹) of the signal for $m_H = 60 - 160$ GeV at $\sqrt{s_{e^+e^-}} = 1(2)$ TeV. Here the acceptance cuts are Eqs. (7), (8) and (9). The discrete backgrounds are calculated using Eq. (10) and the continuum backgrounds are with $m(b\bar{b})$ in between $m_H \pm 5$ GeV. Also we assume NO b -identification, $m_t = 150$ GeV, and the branching fractions of the $V_1, V_2 \rightarrow jj$ are included.

m_H	signal	discrete backgrounds			continuum backgrounds			total	S/\sqrt{B}
	WH	WZ	WW	ZZ	$\bar{t}b\nu$	$e^-g \rightarrow \bar{t}b\nu$	$t\bar{t}e^-$	B	10fb ⁻¹
60	42 (79.5)	0 (0)	0 (0)	0 (0)	0.56 (0.34)	0.18 (0.40)	0.89 (0.67)	1.6 (1.4)	100 (210)
70	40 (77)	0 (0)	0 (0)	0 (0)	0.59 (0.39)	0.12 (0.37)	0.90 (0.74)	1.6 (1.5)	100 (200)
80	38 (74)	0 (0)	250 (490)	0 (0)	0.58 (0.41)	0.10 (0.32)	0.88 (0.72)	250 (490)	7.6 (11)
90	36 (71)	110 (240)	0.14 (0.28)	0.082 (0.036)	0.56 (0.41)	0.083 (0.28)	0.83 (0.70)	110 (240)	11 (14)
100	33 (68)	14 (32)	0 (0)	0.011 (0.0048)	0.52 (0.41)	0.074 (0.24)	0.78 (0.66)	15 (33)	27 (37)
110	30 (63)	0 (0)	0 (0)	0 (0)	0.52 (0.41)	0.055 (0.21)	0.74 (0.62)	1.3 (1.2)	83 (180)
120	25 (54)	0 (0)	0 (0)	0 (0)	0.50 (0.41)	0.045 (0.18)	0.70 (0.58)	1.2 (1.2)	71 (160)
130	19 (41)	0 (0)	0 (0)	0 (0)	0.48 (0.41)	0.040 (0.15)	0.64 (0.53)	1.2 (1.1)	56 (120)
140	12 (26)	0 (0)	0 (0)	0 (0)	0.47 (0.41)	0.034 (0.13)	0.61 (0.51)	1.1 (1.1)	36 (80)
150	5.6 (13)	0 (0)	0 (0)	0 (0)	0.46 (0.40)	0.028 (0.12)	0.55 (0.47)	1.0 (0.99)	17 (41)
160	1.1 (2.6)	0 (0)	0 (0)	0 (0)	0.45 (0.39)	0.021 (0.10)	0.51 (0.46)	0.98 (0.96)	3.5 (8.4)

FIGURES

FIG. 1. Contributing Feynman diagrams for the process $e^- \gamma \rightarrow W^- H \nu$

FIG. 2. Contributing Feynman diagrams for the processes (a) $e^- \gamma \rightarrow W^- Z \nu$, (b) $W^- W^+ e^-$.

FIG. 3. Contributing Feynman diagrams for the processes (a) $e^- \gamma \rightarrow \bar{t} b \nu$, (b) $t \bar{t} e^-$.

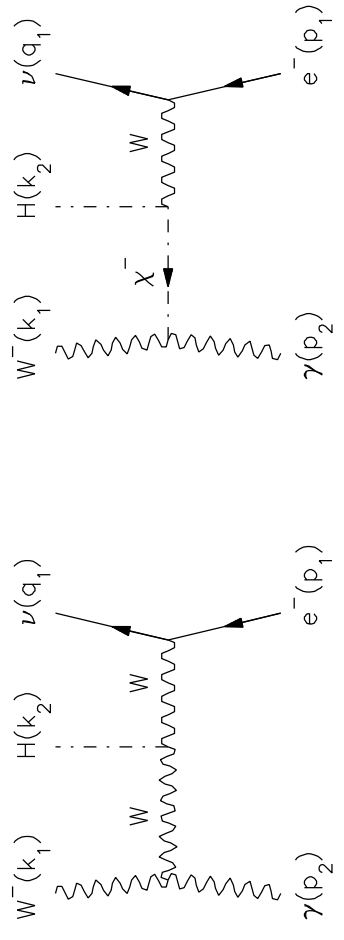
FIG. 4. Total cross sections in pb for signal and various backgrounds versus the center-of-mass energies $\sqrt{s_{e^+e^-}}$ of the parent e^+e^- collider for $m_H = 100$ GeV and $m_t = 150$ GeV before imposing any acceptance cuts. No branching fractions are included. The dash-dotted line represents the resolved photon process for $e^- g(\gamma) \rightarrow \bar{t} b \nu$.

FIG. 5. The dependence of the differential cross section $d\sigma/dp_T(VV)$ on the transverse momentum of the boson-pair for signal and various backgrounds at (a) $\sqrt{s_{e^+e^-}} = 1$ TeV and (b) 2 TeV. NO branching fractions of the boson-pair are included here.

FIG. 6. The dependence of the differential cross section $d\sigma/d\cos\theta_V$ on the cosine of angle between the positive z -axis and the direction of (a) boson V_1 and (b) boson V_2 , and (c) the differential cross-section of $d\sigma/d\cos\theta_{V_1}\cos\theta_{V_2}$ versus $\cos\theta_{V_1}\cos\theta_{V_2}$, at $\sqrt{s_{e^+e^-}} = 1$ TeV. The acceptance cuts are $p_T(VV) > 15$ GeV and central e^- vetoing. NO branching fractions of the boson-pair are included.

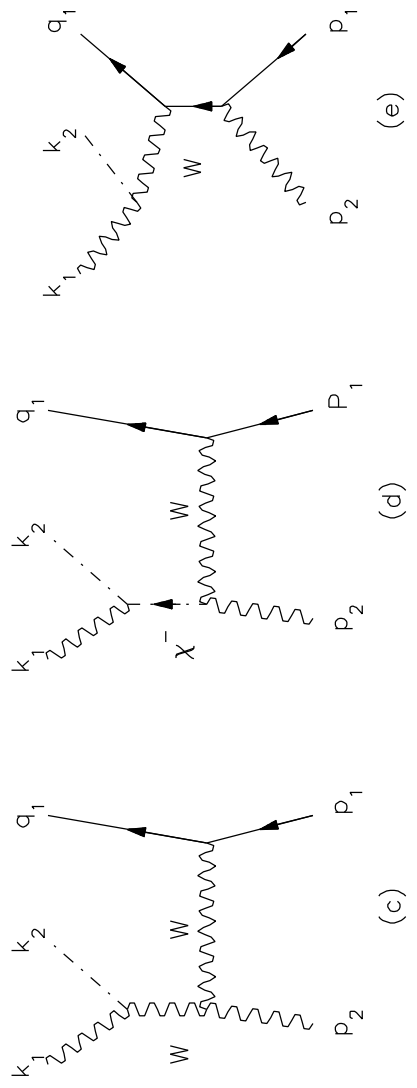
FIG. 7. The dependence of the differential cross section $d\sigma/dm(\bar{b}b)$ on the invariant mass of the $\bar{b}b$ pair (coming from V_2) for the signal and various backgrounds, with the acceptance cuts of $p_T(VV) > 15(30)$ GeV, central electron vetoing and $\cos\theta_{V_1}\cos\theta_{V_2} < 0$, at (a) $\sqrt{s_{e^+e^-}} = 1$ TeV, and (b) 2 TeV. The branching fractions of the $W, Z \rightarrow jj$ and $H, Z \rightarrow \bar{b}b$ are included. We assumed a 100% b -identification.

FIG. 8. The dependence of the differential cross section $d\sigma/dm(jj)$ on the invariant mass of the jj (coming from V_2) pair for the signal and various backgrounds, with the acceptance cuts of $p_T(VV) > 15(30)$ GeV, central electron vetoing and $\cos\theta_{V_1}\cos\theta_{V_2} < 0$, at (a) $\sqrt{s_{e^+e^-}} = 1$ TeV, and (b) 2 TeV. The branching fractions of the $W, Z, H \rightarrow jj$ are included. Here we did NOT assume b -tagging.



(b)

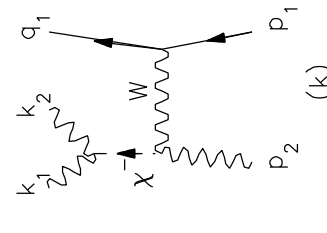
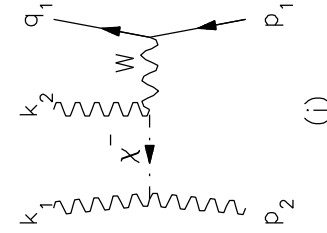
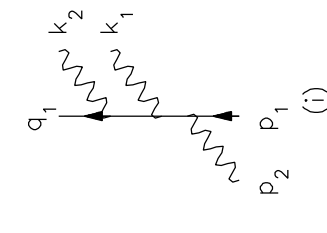
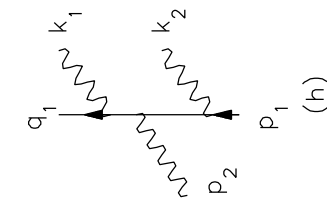
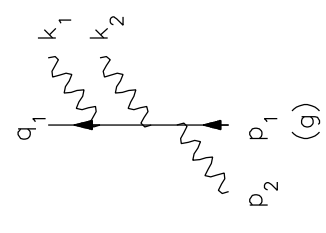
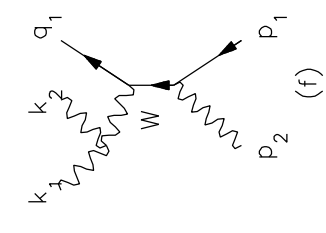
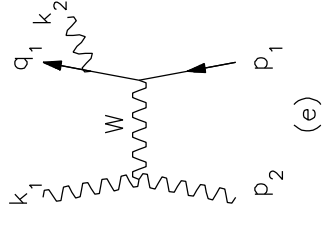
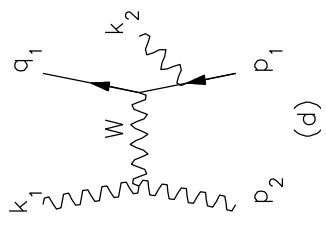
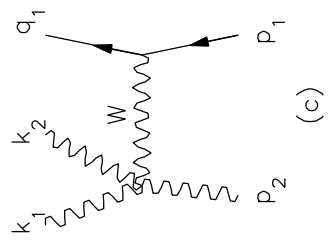
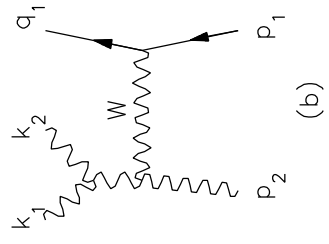
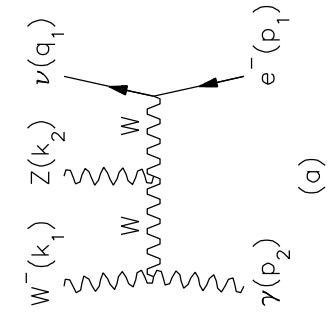
(a)



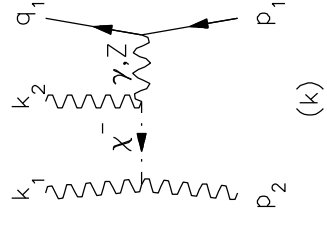
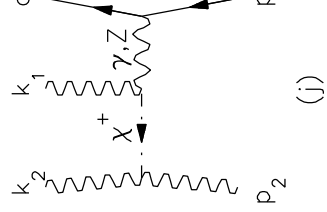
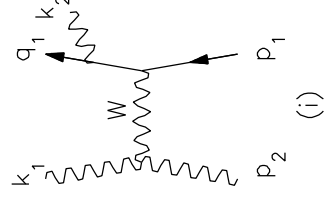
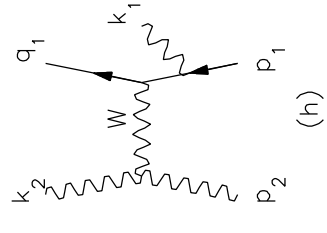
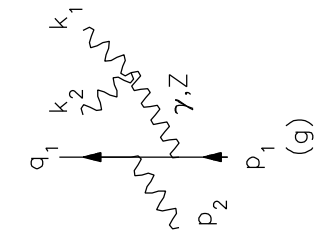
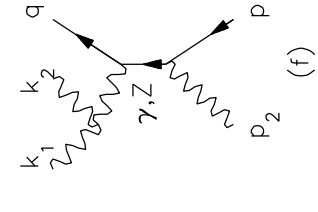
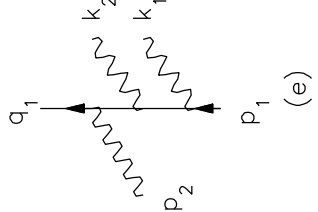
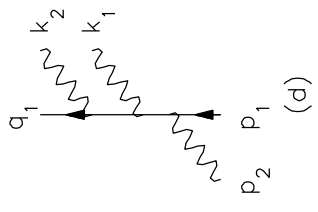
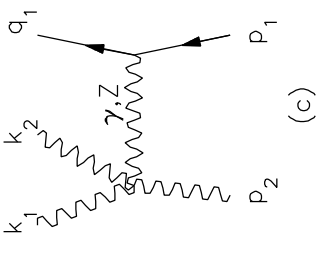
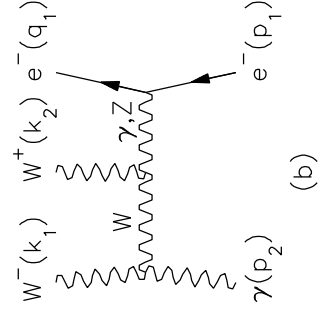
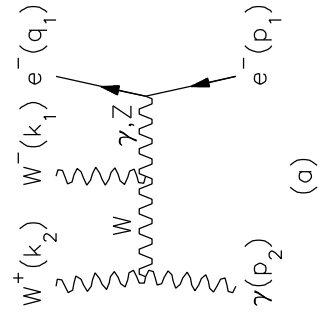
(e)

(d)

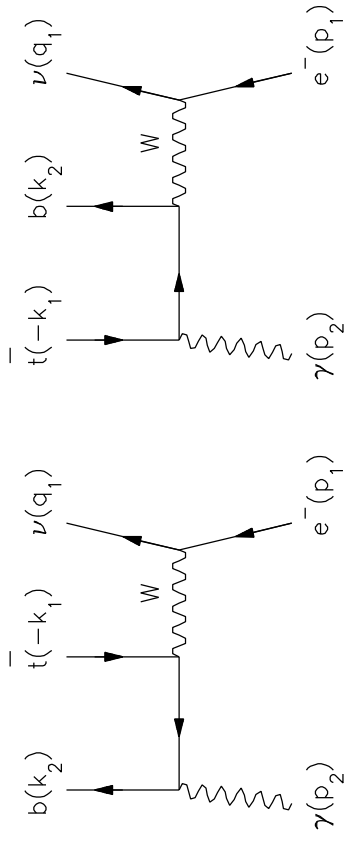
(c)



(a)

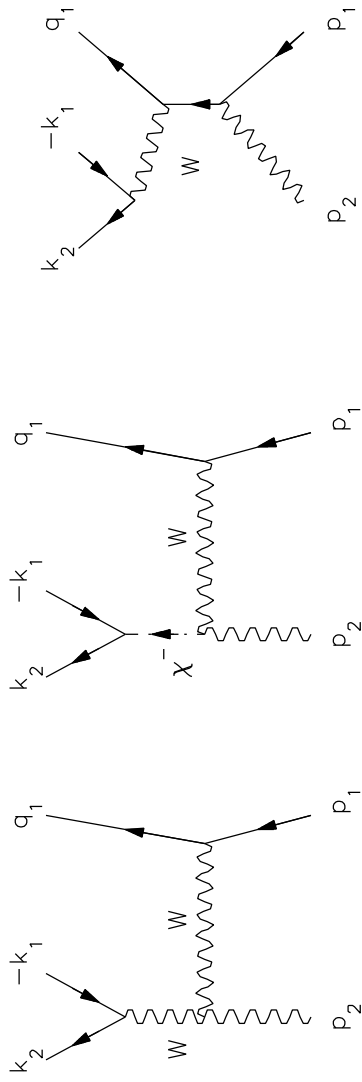


(b)



(a)

(b)

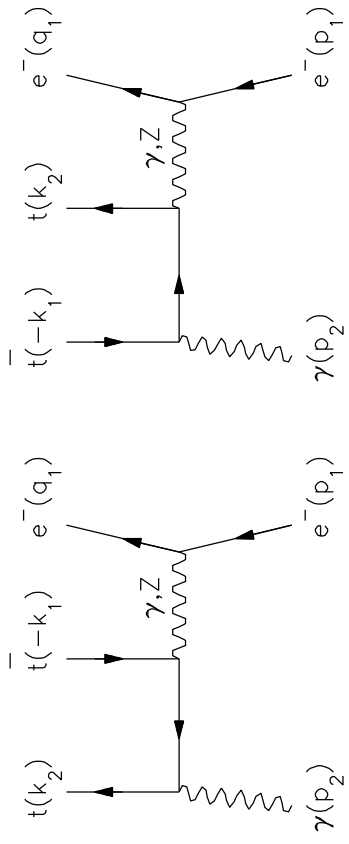


(c)

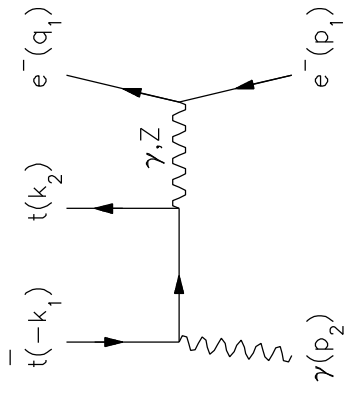
(d)

(e)

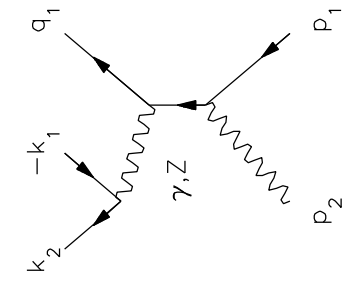
(a)



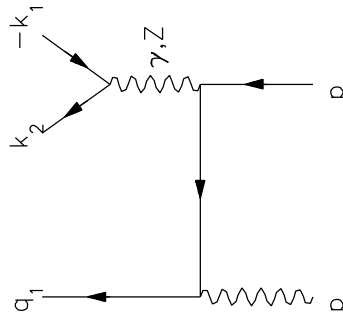
(a)



(b)



(c)



(d)

(b)

